Split-step TLM (SS TLM) : a new scheme for accelerating electromagnetic-field simulation

Sandrick Le Maguer, Alain Peden, Daniel Bourreau, Michel Ney

Split-Step TLM (SS TLM)—A New Scheme for Accelerating Electromagnetic-Field Simulation

Sandrick Le Maguer, Alain Peden, Daniel Bourreau, and Michel M. Ney, *Senior Member, IEEE*

***Abstract*—A new unconditionally stable three-dimensional (3-D) transmisson-line (TLM) algorithm is presented. It is stable regardless of the selected time-step. This new algorithm is based on a split-step theory, whose numerical implementation is given in detail. In addition, the theoretical proof of its unconditional stability is provided. This feature provides some potential advantage for time-domain electromagnetic-field computation as the number of iterations can be arbitrarily reduced for a given space sampling. Unfortunately, it is shown that the numerical dispersion of the new scheme increases when the time-step is different from the maximum value of the standard TLM. However, it is shown that some substantial computer cost reduction can be achieved when irregular meshing is used, as compared to classical 3-D TLM schemes. Thus, a new meshing strategy to improve the scheme accuracy is presented and validated through several examples.**

***Index Terms*—Irregular mesh, split step (SS), transmission-line matrix (TLM), unconditional stability.**

I. Introduction

THE transmission-line matrix (TLM) method is an efficient numerical technique for electromagnetic-field computation [1], [2]. This method is based on a volume discretization of the computational domain and is, hence, well suited for the analysis of arbitrary geometry. As the finite difference time domain (FDTD), the TLM is a time-domain technique that allows wide-band characterization in a single run by applying Fourier transform to time-domain responses. However, the TLM is less dispersive and has the advantage of computing the six-field components at the same location and time. In addition, the TLM is fully compatible with rigorous segmentation techniques [3]. Unfortunately, like FDTD, the TLM is computationally expensive in both CPU time and memory. In particular, this requirement becomes exhaustive when analyzed structures contain fine details. Indeed, in that case, graded mesh is usually used to reduce memory requirement. As a result, the time-step is reduced in proportion to the smallest cell size and, correspondingly, the amount of iterations.

The symmetrical condensed node (SCN) is the basic three-dimensional (3-D) TLM cell (or node). It was introduced by Johns in 1987 [4] and requires the storage of 18 voltage values since much effort has been driven to decrease the computer cost of this numerical scheme. For instance, two new nodes: the hybrid SCN (HSCN: 15 voltages) [5], [6] and the super SCN (SSCN: 12 voltages) [7] were proposed. Also, these nodes provide some advantage in term of the time-step while using a graded mesh. Nevertheless, there exist a maximum time-step value to enforce stability. Note that several accelerating procedures for the above schemes have been proposed. They are listed and compared in [8].

A major improvement in memory reduction was the creation of the alternating TLM scheme (ATLM) [9]. This model allows the use of any type of TLM node while decreasing the computational effort by a factor of two. Unfortunately, this technique has a major drawback: boundaries have to be placed at the center of the TLM cell. This condition breaks the generality of the TLM scheme since special nodes have to be created for each type of boundary. This technique was also associated with the rotated TLM (RTLM) [10], which leads to another 50% computer-cost reduction. With the same objective, the alternating rotated TLM (AR-TLM) scheme was proposed [11]. However, boundary treatment in some configurations has not yet been solved.

Recently, a new FDTD scheme without a maximum time-step limit was proposed [i.e., alternating-direction implicit FDTD (ADI FDTD)]. First implemented as a two-dimensional (2-D) scheme by Namiki [12], it was then extended to 3-D by Zheng *et al.* [13]. Such a scheme has significant advantage in simulations involving a graded mesh [14]. Alternating-direction implicit (ADI) schemes were implemented for the TLM [15]–[17]. However, it was found in [15] that ADI schemes were not appropriate for implementation to TLM since some time-step ambiguity remains.

In this paper, a new approach to implement such a type of unconditionally stable algorithm is presented. This technique, called split-step (SS), is then applied to 3-D TLM and numerical implementation is given in details. It is shown that the memory requirement per cell is divided by a factor of three. In addition, it is shown that the numerical scheme is unconditionally stable for any time-step. A short study of the numerical dispersion leads to imposing a meshing strategy that takes advantage of using a larger time-step while keeping the numerical dispersion error negligible.

II. Scheme Derivation

A. ADI-FDTD Technique

The ADI-FDTD scheme is a two-step algorithm, which leads to a semi-implicit method by approximating Maxwell's equations in a convenient manner. Let us describe the ADI approxi-

The authors are with the Groupe des Ecoles de Télécommunications, Département Micro-Ondes, Centre National de la Recherche Scientifique, Laboratoire d'Electronique et des Systèmes de Telecommunication, Ecole Nationale Supérieure des Télécommunications de Bretagne, 29238 Brest Cedex 3, France (e-mail: sandrick.lemaguer@enst-bretagne.fr).

mation of the Maxwell–Ampère equation for the temporal variation of the E_x-component. First, the usual iterative scheme is subsequently applied in time as follows.

First step:

$$\varepsilon_x\varepsilon_0 \left.\frac{\partial E_x}{\partial t}\right)_n + \sigma_{ex}E_x)_n = \left.\frac{\partial H_z}{\partial y}\right)_{n-(1/2)} - \left.\frac{\partial H_y}{\partial z}\right)_{n+(1/2)}. \tag{1}$$

Second step:

$$\varepsilon_x\varepsilon_0 \left.\frac{\partial E_x}{\partial t}\right)_{n+1} + \sigma_{ex}E_x)_{n+1} = \left.\frac{\partial H_z}{\partial y}\right)_{n+(3/2)} - \left.\frac{\partial H_y}{\partial z}\right)_{n+(1/2)} \tag{2}$$

where n is the time-step index, ε_0 is the permittivity of free space, ε_x is the relative permittivity in the x-direction, and σ_{ex} is the electric losses along the same direction. As shown, the time derivative is approximated at $n\Delta t$ (Δt being the time-step), while spatial derivatives are approximated at $(n-1/2)\Delta t$ and $(n+1/2)\Delta t$. This step is then followed by a step where the time derivative is approximated at $(n+1)\Delta t$, while spatial derivatives are approximated at $(n+1/2)\Delta t$ and $(n+3/2)\Delta t$. These time shifts are the basis of the ADI process. It can be demonstrated that the finite-difference approximation of (1) and (2) using Yee's grid [18] leads to an unconditionally stable algorithm [12], [13].

B. SS Technique and Its TLM Implementation

As mentioned before, ADI is not advantageously applicable to the TLM. A similar approach based on SS theory [19] is used instead, as its numerical implementation is simpler. It consists of splitting a 3-D phenomenon in successive sub-one-dimensional (1-D) phenomena. To achieve this, a modification of the time-sampling procedure in Maxwell's field equations has to be carried out. The technique splits the basic equations into two successive steps. For instance, the time dependence of the x electric-field component E_x given by the Maxwell-Ampère equation is divided into the following two equations:

$$\frac{1}{2}\left(\varepsilon_x\varepsilon_0\frac{\partial E_x}{\partial t} + \sigma_{ex}E_x\right) = \frac{\partial H_z}{\partial y} \tag{3}$$

$$\frac{1}{2}\left(\varepsilon_x\varepsilon_0\frac{\partial E_x}{\partial t} + \sigma_{ex}E_x\right) = -\frac{\partial H_y}{\partial z}. \tag{4}$$

According to the theory of split algorithms, (3) and (4) have to be solved subsequently in the iterative process to obtain unconditional stability. Furthermore, to get a coherent spatial mapping of field components, the scheme is divided into the following two steps.

- Step 1) An approximation of (3) between $(n-1/2)\Delta t$ and $n\Delta t$ is obtained followed by an approximation of (4) between $n\Delta t$ and $(n+1/2)\Delta t$.
- Step 2) An approximation of (4) between $(n+1/2)\Delta t$ and $(n+1)\Delta t$ is obtained followed by an approximation of (3) between $(n+1)\Delta t$ and $(n+3/2)\Delta t$.

The above approximations are performed using the approach proposed by Peña and Ney [20]: from field component sample to arm-voltage correspondences, enforcement of curl's Maxwell's equations lead to relationships between reflected voltages and total fields at the node center. This approach can also be used with Maxwell's equation derivatives. For example, let us approximate (3) between $(n-1/2)\Delta t$ and $n\Delta t$ using the TLM grid. Field samples on this grid in the (yoz)-plane of the Cartesian grid are depicted in Fig. 1.

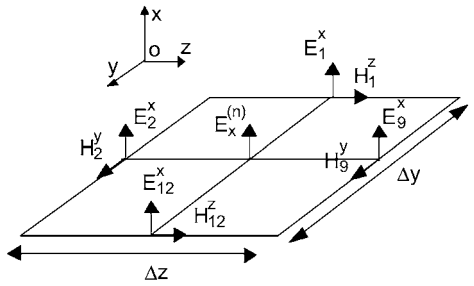

Fig. 1. 3-D TLM fields samples in the (yoz)-plane with respect to Johns' notation [4].

Using the finite-difference approximation of time and space derivatives in (3) leads to

$$\frac{\varepsilon_x}{\Delta x\Delta t c_0 Z_0}\Delta x\left(E_x^n - E_x^{(n-(1/2))}\right) + \frac{\sigma_{ex}}{2\Delta x}\Delta x E_x^n = \left(\frac{H_{12}^z - H_1^z}{\Delta y}\right)^{(n-(1/2))} \tag{5}$$

where c_0 is the speed of light in vacuum and Z_0 is the impedance of free space. Δx, Δy, and Δz are the cell size for each direction of the Cartesian grid. $E_x^{(n)}$ is the x-field component at the center of the cell at $n\Delta t$. H_1^z denotes a field component (in this case, z-component) on the face of the cell, which corresponds to port 1 with respect to Johns' notation [4]. It should be stressed that, in (5), $E_x^{(n)}$ is unknown and that field components are known on the faces of the cell at $(n-1/2)\Delta t$. Thus, to solve (5), one can enforce

$$E_x^{(n-(1/2))} = \frac{1}{2}\left(E_1^x + E_{12}^x\right)^{(n-(1/2))} \tag{6}$$

which is an average comparable to those usually used in the TLM schemes' derivation (for instance, see [20]). Injecting (6) in (5) leads to

$$2\frac{\Delta x E_x^n}{A_{ex}} = \Big[\left(\Delta x E_1^x - Z_{ex}\Delta z H_1^z\right) + \left(\Delta x E_{12}^x + Z_{ex}\Delta z H_{12}^z\right)\Big]^{(n-(1/2))} \tag{7}$$

where $A_{ex} = 4/(4+R_{ex})$, $R_{ex} = Z_0 s(\sigma_{ex}/\varepsilon_x)$, $Z_{ex} = Z_0\bar{C}_x$, $\bar{C}_x = (s\Delta x/\varepsilon_x\Delta y\Delta z)$, and $s = 2c_0\Delta t$.

The same approximation is applied from $n\Delta t$ to $(n+1/2)\Delta t$ to (4) that yields

$$2\frac{\Delta x E_x^n}{A'_{ex}} = \Big[\left(\Delta x E_2^x - Z_{ex}\Delta y H_2^y\right) + \left(\Delta x E_9^x + Z_{ex}\Delta y H_9^y\right)\Big]^{(n+(1/2))} \tag{8}$$

where $A'_{ex} = 4/(4-R_{ex})$.

Applying the same procedure to the other scalar differential equations derived from Maxwell's curl equations, one can obtain the complete set of updating equations provided in the Appendix.

One can note from (7) and (8) that the combination of fields on the faces of the cell corresponds to the usual TLM voltages. For example, the reflected voltage on port 2 of the SCN is usually defined as

$$V_2^r = \frac{1}{2}\left(\Delta x E_2^x - Z_0 \Delta y H_2^y\right) \tag{9}$$

because the impedance of this port is Z_0 [4]. Hence, the voltage notation is not maintained here because corresponding arm impedances are not the same depending on what field component is evaluated at the center of the cell. For example, from (A.7) and (A.11) (see the Appendix), it can be seen that port 2 has two different characteristic impedances at the same time. Thus, the voltage notation is no longer unified and one has to work directly with field components. Furthermore, arm impedances can never be zero or negative. Thus, from a TLM point-of-view, the scheme appears to be unconditionally stable. This point will be theoretically proven in Section III.

From (7), it can be seen that the field value at the center of the cell can be easily calculated from tangential-field components on the faces at the previous half time-step. However, a problem arises when one tries to estimate those tangential-field components from fields at the center at the previous half time-step [see (8)]. Considering an isolated cell, one has to solve a system of six equations with 12 unknowns. Consequently, this part of the scheme has to be solved by taking into account the neighboring cells. As for ADI FDTD, this procedure leads to an implicit solution step of the algorithm.

To illustrate this point, consider a part of a computational volume that consists of three adjacent cells only distributed along the z-direction (see Fig. 2). The space is limited by two perfect electric conductors (PECs).

Using (A.7) and (A.11) in the lossless case (i.e., $A'_{ex} = 1$ and $A'_{my} = 1$), one obtains the following linear system of equations:

$$\begin{bmatrix}
1 & 0 & 0 & 0 & 0 & 0 & 0 & 0 \\
1 & -Z_{ex}^{(1)} & 1 & Z_{ex}^{(1)} & 0 & 0 & 0 & 0 \\
-1 & Z_{my}^{(1)} & 1 & Z_{my}^{(1)} & 0 & 0 & 0 & 0 \\
0 & 0 & 1 & -Z_{ex}^{(2)} & 1 & Z_{ex}^{(2)} & 0 & 0 \\
0 & 0 & -1 & Z_{my}^{(2)} & 1 & Z_{my}^{(2)} & 0 & 0 \\
0 & 0 & 0 & 0 & 1 & -Z_{ex}^{(3)} & 1 & Z_{ex}^{(3)} \\
0 & 0 & 0 & 0 & -1 & Z_{my}^{(3)} & 1 & Z_{my}^{(3)} \\
0 & 0 & 0 & 0 & 0 & 0 & 1 & 0
\end{bmatrix}
\times
\underbrace{\begin{bmatrix}
\Delta x E_x^{(a)} \\ \Delta y H_y^{(a)} \\ \Delta x E_x^{(b)} \\ \Delta y H_y^{(b)} \\ \Delta x E_x^{(c)} \\ \Delta y H_y^{(c)} \\ \Delta x E_x^{(d)} \\ \Delta y H_y^{(d)}
\end{bmatrix}^{(n+(1/2))}}_{\text{field components on the faces (unknowns)}}
=
\underbrace{\begin{bmatrix}
0 \\
2\Delta x E_x^{(1)} \\
\frac{2Z_0}{\bar{D}_y}\Delta y H_y^{(1)} \\
2\Delta x E_x^{(2)} \\
\frac{2Z_0}{\bar{D}_y}\Delta y H_y^{(2)} \\
2\Delta x E_x^{(3)} \\
\frac{2Z_0}{\bar{D}_y}\Delta y H_y^{(3)} \\
0
\end{bmatrix}^{(n)}}_{\text{field components at the centers of the cells (known)}} . \tag{10}$$

In (10), the superscripts indicate either the cell or face numbers given in Fig. 2. Note that the first and last lines of (10) pertain to boundary conditions. Thus, for the case discussed here, the electric-field components that are tangent to perfect conductors are set to zero. Also, note that, as for classical TLM schemes, the SS TLM can straightforwardly simulate a wide range of boundary conditions (perfect magnetic, impedance, etc.). To solve the above system, one has to invert the above matrix that yields the tangential-field components on the faces as a function of fields at the center of all cells along the z-direction.

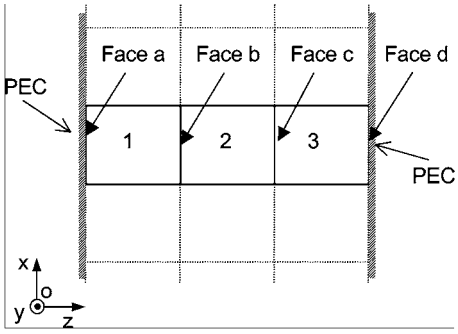

Fig. 2. Illustration of the implicit solution step in the case of three adjacent cells along the z-direction.

It is worth noting that this matrix is inverted only once and stored before the time iterations start. Thus, for one z-directed line through the space lattice, the field on the faces are calculated at $(n+1/2)\Delta t$ directly followed by the calculation of field at the center at $(n+1)\Delta t$ using the updated (B.1) and (B.5). Hence, only the six field components at the center need to be stored. This represents a memory gain of a factor of three compared to the classical 3-D TLM scheme. The above implicit procedure must be repeated for each z-cut through the grid and repeated for all x- and y-cuts. The whole SS TLM scheme is described in Fig. 3.

One should note that the amount of multiplications and additions is much larger than for the classical TLM scheme. This drawback is essentially due to the use of an inverted matrix to calculate fields on the faces of the cell [see (10)]. However, it should be stressed that the potential advantage brought by the SS TLM scheme resides in the case of irregular mesh where the time-step imposed by the smallest mesh size need not be enforced with the SS TLM.

III. Stability Analysis of SS TLM Scheme

As seen in Section II, impedances of the new SS TLM can never be negative. It indicates that the scheme appears to be unconditionally stable. The theoretical proof of this assertion is given below.

The new scheme can be written recursively as follows:

$$\vec{X}^{n+(3/2)} = M\vec{X}^{n-(1/2)}$$

with

$$\vec{X}^{n-(1/2)} = \begin{bmatrix}
\Delta x E_x \\ \Delta y E_y \\ \Delta z E_z \\ \Delta x H_x \\ \Delta y H_y \\ \Delta z H_z
\end{bmatrix}^{(n-(1/2))} . \tag{11}$$

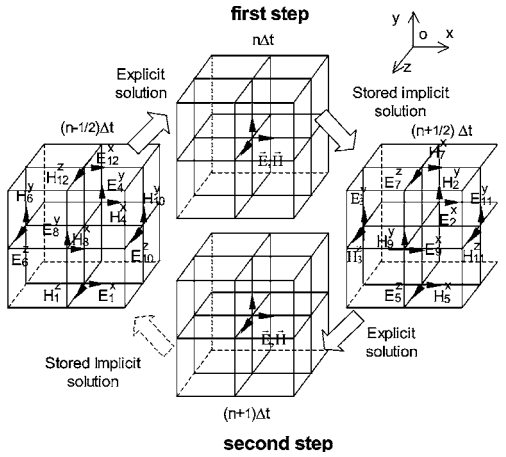

Fig. 3. Illustration of the SS TLM algorithm.

The stability of such a scheme can be proven using the Fourier method described in [19] and used in [13] to prove ADI-FDTD stability. The field components are represented in the spatial spectral domain. The eigenvalues of the matrix M are then determined. Stability is ensured if they are located within or on the limit of the unit circle in the complex plane.

Let us assume that k_x, k_y, and k_z are the spatial frequencies along the x-, y-, and z-directions. Thus, field components in the spatial spectral domain can be expressed, for example, as

$$E_2^x)^n = E_x^n e^{-j(k_x i\Delta x + k_y j\Delta y + k_z(k-(1/2))\Delta z)} \quad (12a)$$

$$H_2^y)^n = H_y^n e^{-j(k_x i\Delta x + k_y j\Delta y + k_z(k-(1/2))\Delta z)} \quad (12b)$$

where i, j, and k are the indexes of the coordinates of the center of the cell.

Both steps of the SS TLM can be written in the matrix form

$$P_1\vec{X}^{n+(1/2)} = Q_1\vec{X}^{n-(1/2)} \quad (13a)$$

for the first step. The second step is

$$P_2\vec{X}^{n+(3/2)} = Q_2\vec{X}^{n+(1/2)} \quad (13b)$$

where P_1 and P_2 correspond to the implicit procedures, while Q_1 and Q_2 correspond to the explicit parts of the algorithm. Their expressions are obtained by injecting the expressions of the type (12) into (A.1)–(A.12) and (B.1)–(B.12). For example, the first line of P_1 and Q_1 is obtained by substituting expressions of fields on the faces such as (12) in (A.1) and (A.7), which leads to

$$\begin{aligned} A_{ex}&\left[\Delta x E_x^{(n-(1/2))}\cos\left(\frac{k_y}{2}\Delta y\right)\right. \\ &\left. -jZ_{ex}\Delta z H_z^{(n-(1/2))}\sin\left(\frac{k_y}{2}\Delta y\right)\right] \\ &= A'_{ex}\left[\Delta x E_x^{(n+(1/2))}\cos\left(\frac{k_z}{2}\Delta z\right)\right. \\ &\left. -jZ_{ex}\Delta y H_y^{(n+(1/2))}\sin\left(\frac{k_y}{2}\Delta y\right)\right]. \end{aligned} \quad (14)$$

By substituting (13a) in (13b), the following expression is then found:

$$\vec{X}^{n+(3/2)} = P_2^{-1}Q_2P_1^{-1}Q_1\vec{X}^{n-(1/2)} = M\vec{X}^{n-(1/2)}. \quad (15)$$

The eigenvalues λ of M are found by solving the equation

$$\det(M-\lambda I) = 0 \quad (16)$$

where I is the identity matrix. Condition (16) yields

$$(\lambda-1)^2\left(\lambda^2+A\lambda+1\right)^2 = 0 \quad (17)$$

TABLE I
CPU EXPENDITURE OF SS TLM COMPARED WITH TLM

Algorithm	CPU (s)	Gain compared to TLM
SCN-TLM	146	1.0
SS-TLM	1370	9.65
SS-TLM block	1285	9.05
SS-TLM band	769	5.42
SS-TLM tri-diagonal	186	1.31

with

$$A = 2\frac{U+W-\left(s^3S_xS_yS_z\right)^2-64\varepsilon_r^3\mu_r^3\left(\Delta xC_x\Delta yC_y\Delta zC_z\right)^2}{V}$$

$$W = 4\varepsilon_r\mu_r s^4\left(W_x+W_y+W_z\right)$$

$$U = \left(4\varepsilon_r\mu_r s\right)^2\left(U_x+U_y+U_z\right)$$

$$V = V_xV_yV_z$$

$$W_i = \left(\Delta iC_iS_jSk\right)^2$$

$$U_i = \left(\Delta jC_j\Delta kC_kS_i\right)^2$$

with $(i,j,k) \in \{(x,y,z),(z,x,y),(y,z,x)\}$

$$V_i = \left(sS_i\right)^2 + 4\varepsilon_r\mu_r\left(\Delta iC_i\right)^2$$

$$S_i = \sin\left(\frac{k_i\Delta i}{2}\right)$$

and

$$C_i = \cos\left(\frac{k_i\Delta i}{2}\right)$$

with

$$i \in (x,y,z).$$

Note that, without loss of generality, the medium is considered isotropic ($\varepsilon_r = \varepsilon_x = \varepsilon_y = \varepsilon_z$ and $\mu_r = \mu_x = \mu_y = \mu_z$) and lossless. From (17), it can be seen that there are six eigenvalues. Two of them correspond to the static solution ($\lambda_1 = \lambda_2 = 1$), while the others pertain to the propagating solutions. Each of them has a magnitude of unity, which implies that the SS TLM is unconditionally stable. There is no more maximum time-step. Last, but not least, the above conclusion proves that, unlike the standard TLM, the SS TLM algorithm does not generate spurious solutions.

IV. ACCELERATING PROCEDURES

As explained before, the SS TLM algorithm requires some overhead in computer expenditure due to the implicit part of the technique. However, the matrix involved in (10) is very sparse since it is a band matrix. Thus, dedicated accelerating procedures can be used. For instance, the software NAG FORTRAN Library[1] provides routines adapted to block diagonal matrices (referred to as F04LHF), band matrices (referred to as F07BEF), and tri-diagonal matrices (referred to as F04LEF) since the matrix in (10) can easily be rearranged in a tri-diagonal form. The CPU expenditure was tested for a 3-D $50\times50\times50$ cells volume and compared to the classical TLM. Results are presented in Table I. One can observe that the routine for a tri-diagonal matrix is really efficient and reduces the overall CPU time overhead to only 30%. Furthermore, this overhead remains the same whatever the size of the problem

[1]NAG FORTRAN Library, Mark 19, Numerical Algorithm Group.

treated is. This is due to the fact that the tri-diagonal procedure CPU time increases linearly with the amount of cells, just as the TLM does.

In conclusion, directly using the inverted matrix is around ten times longer than the classical TLM, which balance any available advantage of the SS TLM algorithm. However, if specific procedures are used such as a band matrix or tri-diagonal matrix, the CPU time becomes comparable to the SCN TLM. Hence, the SS TLM is only slightly slower than the usual TLM schemes while providing the advantage of using an arbitrary time-step. This aspect will be discussed in more details in Section V.

V. Numerical Results

A. Comparison Between SS TLM and Standard TLM

The new SS TLM scheme was tested and compared to the SCN TLM [4] in the case of a cavity made of an empty short-circuited rectangular waveguide (20×10 mm cross section) with 50-mm total length. The cavity is excited so that TE_{10k} modes resonate. The relative error is given by

$$e(\%) = \frac{f_s - f_{\mathrm{th}}}{f_{\mathrm{th}}} \tag{18}$$

where f_s is the simulated resonance frequency of the modes and f_{th} is the theoretical one. Fig. 4 shows the error as a function of cell size to wavelength ratio for different time-steps. The total time of the simulation is 16.7 ns. It means that the amount of iterations depends on the time-step chosen to perform the simulation.

It is observed that when the maximum time-step of the SCN TLM ($\Delta t_{\max}$) is used, no difference appears between the two schemes. Thus, the strict equivalence between both can be proven theoretically at this maximum time-step value (see [21]). In addition, it is noted that, at $\Delta t_{\max}$, the error is below 0.1% up to the acceptable dispersion limit $\Delta l/\lambda = 0.1$ for both schemes. It is well known that numerical dispersion is minimum at a maximum time-step with the SCN TLM. This feature still holds for the SS TLM. Furthermore, when the time-step decreases, the dispersion error increases for both schemes. However, it can be observed from Fig. 4 that the error produced by the SS TLM is larger than the one produced by the SCN TLM.

B. Numerical Dispersion of SS TLM as a Function of Time-Step ($\Delta t > \Delta t_{\max}$)

In spite of the high accuracy of the SS TLM at the SCN TLM maximum time-step, one has to consider the evolution of the dispersion error, especially when using a larger time-step.

For this purpose, a simulation under the same conditions as used in Fig. 4 is performed, but for several $\Delta t > \Delta t_{\max}$ (values for which the SCN TLM would be instable). As in a classical TLM, the numerical dispersion of the SS TLM increases with $\Delta l/\lambda$ (see Fig. 5). However, if $\Delta t > \Delta t_{\max}$, the error increases very rapidly with the relative cell size, as compared to cases with $\Delta t < \Delta t_{\max}$ (see Fig. 4).

Therefore, the advantage of using an arbitrary larger time-step for the SS TLM is greatly reduced by the numerical dispersion increase. However, by examining Fig. 5, a significant advantage

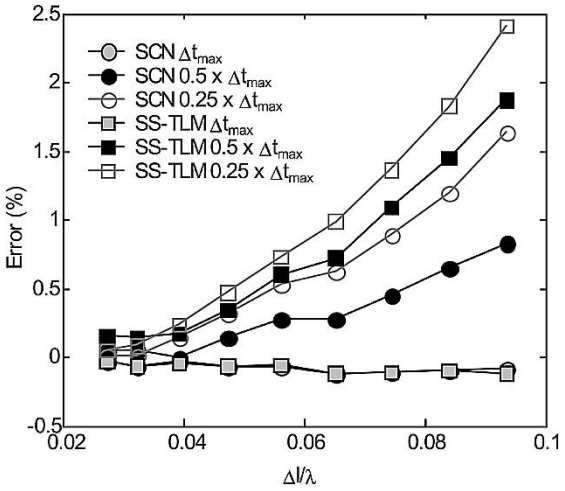

Fig. 4. Error on resonance frequencies (markers) obtained in a rectangular cavity. Comparison between the SS TLM and SCN TLM ($\Delta t_{\max}$ is the maximum time-step of the SCN TLM) with cubic cells (i.e., $\Delta l = \Delta x = \Delta y = \Delta z = 1$ mm).

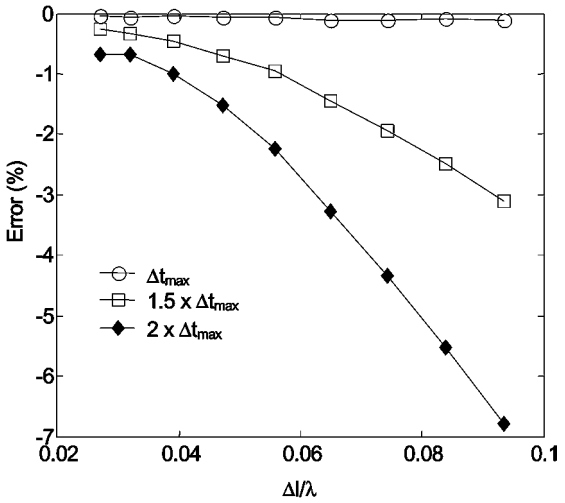

Fig. 5. Error on resonance frequencies (markers) of an empty rectangular cavity. Simulations are performed for several time-steps with the SS TLM ($\Delta t_{\max}$ is the classical TLM maximum time-step).

can be gained when irregular meshing is used, as is explained below.

Usually, when using a variable mesh, one has to impose to the whole meshing the lowest time-step typically enforced by considering the smallest cell dimension. This implies a large amount of iterations to obtain a nontruncated time response. In the case of the SS TLM, one can use $\Delta t_{\max}$ for which dispersion is minimum. As a result, large cells will produce negligible velocity error up to the standard limit $\Delta l/\lambda \sim 0.1$ (see the example in Fig. 5). On the other hand, small cells will be processed with a time-step much larger than $\Delta t_{\max}$, but with very low values of $\Delta l/\lambda$. As can be observed in Fig. 5, ratios below 0.03 implies a negligible dispersion error. Thus, the choice of a maximum standard TLM time-step acts like a compromise between the time-step and numerical error in each region of the mesh. As a result, the time-step used in the SS TLM can be much larger than the time-step used in a classical TLM for an irregular mesh, and substantial gain in terms of the CPU time is expected.

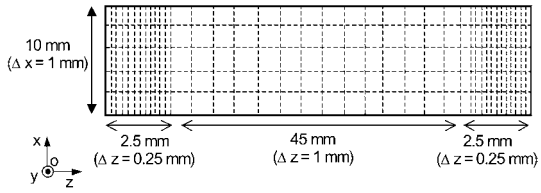

Fig. 6. Geometry of the variable mesh used in a rectangular cavity to test the new meshing strategy.

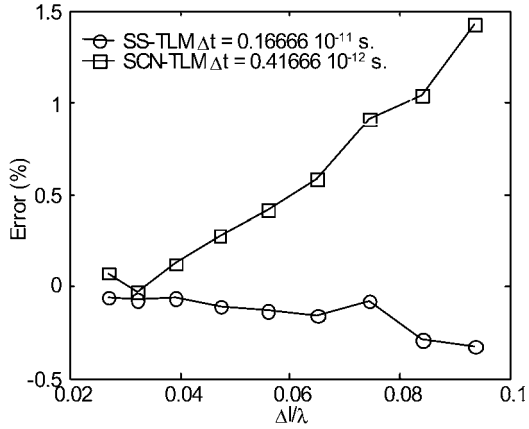

Fig. 7. Error on resonance frequencies (markers) of an empty rectangular cavity with a variable mesh (Fig. 6). Comparison between the SS TLM mesh strategy and the SCN TLM.

The above meshing strategy was tested and compared to the SCN TLM. The geometry is the same as in Figs. 4 and 5, except that the mesh density in the longitudinal direction is increased by a factor of four at each extremity of the cavity, as depicted in Fig. 6. Consequently, the maximum time-step of the SCN TLM is four times smaller than for the SS TLM selected time-step. This means that the amount of iteration with the SS TLM is four times smaller. From previous observations, the overall cost for the SS TLM analysis is three times faster than with SCN TLM computations.

As observed in Fig. 7, the reduction of numerical dispersion with the SS TLM is maintained. Consequently, error does not exceed 0.4%. On the other hand, since the time-step of the SCN TLM is smaller, the numerical dispersion increases in the large-cell regions. As a result, the error obtained can be larger than 1.4%. This experiment validates the new SS TLM mesh strategy. It should be noted that, if accuracy is maintained, the CPU time is decreased. However, this technique has to be experimented with more complex structures to ascertain the above conclusion.

C. Frequency-Selective Surface (FSS) Simulation

Finally, the SS TLM and conventional TLM are compared by simulating an FSS at millimeter wavelength. A quasi-optical test bench developed at the Laboratoire d'Electronique et des Systèmes de Telecommunication (LEST), Brest, France [22] is used to measure S-parameters. The screen under test is composed of a dielectric substrate ($\varepsilon_r = 2.2$) with a 2-D periodical square metallization. Since the wave impinges at normal incidence (perpendicular to periodicity directions), the simulation can be reduced to one-quarter of a single motive by properly choosing boundary conditions, as shown in Fig. 8. Perfect magnetic walls are used in the (yoz)-planes and perfect electric walls in the (zox)-planes to limit the computational volume. The structure is excited by a plane wave with a polarization in the y-direction. In addition, PML absorbing boundary conditions (ABCs) are used at both ends of the computational domain to simulate free space [23]. The total volume simulated is composed of $30 \times 30 \times 120$ cells and a variable mesh is used around the metal edges to decrease the coarseness error. The reflection coefficients obtained with the SS TLM and SCN TLM are shown in Fig. 9, in which they are compared to measurements.

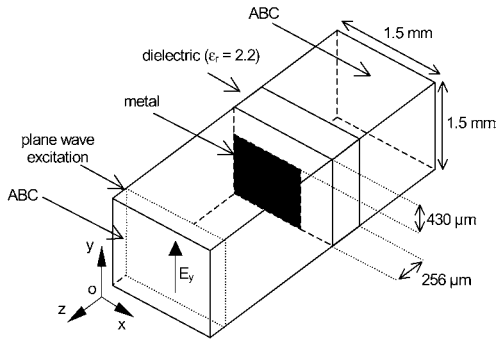

Fig. 8. Geometry of the simulation performed to characterize an FSS (basic cell: $\Delta l = 63.5\ \mu$m).

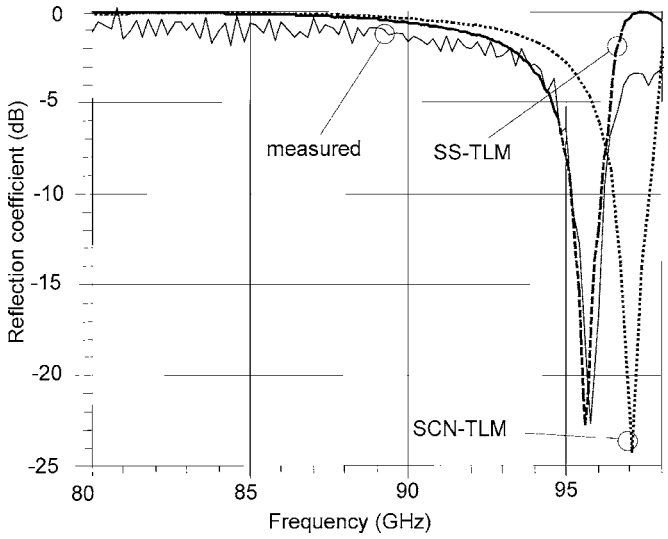

Fig. 9. Reflection coefficient obtained with the FSS depicted in Fig. 8. Comparison between the SS TLM, TLM, and measurements.

At first glance, the SS TLM seems more accurate than the SCN TLM. However, as losses were not included in the simulation, a slight downward frequency shift is usually expected when they are taken into account. Therefore, the TLM and SS TLM should provide comparable accuracy around 1% in terms of frequency.

It should also be mentioned that the comparison with measurements are shown up to 98 GHz. The reason is that a higher order mode (referred to as Floquet modes or grating modes [24]) is generated around 100 GHz. Since simulated S-parameters were extracted considering single-mode propagation, the comparison with measurements would be meaningless.

Finally, note that by using the meshing strategy described in the Section IV, the SS TLM simulation is performed 3.4 times faster than the conventional TLM with a three-factor memory storage reduction, confirming SS TLM advantages.

VI. Conclusion

A new approach to obtain an unconditionally stable algorithm has been presented and implemented in a 3-D TLM form. Based on SS theory, the SS TLM includes two subsequent time operations in the time iterative scheme. Consequently, the memory storage per cell is divided by a factor of three. The stability of the new algorithm is theoretically proven and it is found that spurious modes inherent to the classical TLM no longer exist. However, like the ADI FDTD, the SS TLM involves an implicit solution procedure to be performed before time iterations start. It is shown that the overall CPU time ratio SS TLM over a standard TLM does not exceed 1.3.

Numerical results confirm that at the maximum time-step, the new scheme and classical SCN TLM are equivalent. As observed in FDTD, the numerical dispersion of the new method increases with the time-step. However, unlike the ADI FDTD, for which numerical dispersion continuously increases with the time-step, the numerical dispersion of the SS TLM is minimal at the SCN TLM maximum time-step. From this observation, a new meshing strategy for irregular meshing is proposed and tested. Results show that, while keeping dispersion error at a negligible level, some substantial gain in terms of overall computer expenditure is obtained with the SS TLM.

Appendix

The complete SS TLM updating equations are listed here for both time-steps.

First step:

Explicit part (from $(n-1/2)\Delta t$ to $n\Delta t$):

$$2\Delta x E_x^{(n)} = A_{ex}\left[\left(\Delta x E_1^x - Z_{ex}\Delta z H_1^z\right) + \left(\Delta x E_{12}^x + Z_{ex}\Delta z H_{12}^z\right)\right]^{(n-(1/2))} \tag{A.1}$$

$$2\Delta y E_y^{(n)} = A_{ey}\left[\left(\Delta y E_4^y - Z_{ey}\Delta x H_4^x\right) + \left(\Delta y E_8^y + Z_{ey}\Delta x H_8^x\right)\right]^{(n-(1/2))} \tag{A.2}$$

$$2\Delta z E_z^{(n)} = A_{ez}\left[\left(\Delta z E_6^z - Z_{ez}\Delta y H_6^y\right) + \left(\Delta z E_{10}^z + Z_{ez}\Delta y H_{10}^y\right)\right]^{(n-(1/2))} \tag{A.3}$$

$$2Z_0\frac{\Delta x H_x^{(n)}}{\bar{D}_x} = A_{mx}\left[\left(\Delta y E_8^y + Z_{mx}\Delta x H_8^x\right) - \left(\Delta y E_4^y - Z_{mx}\Delta x H_4^x\right)\right]^{(n-(1/2))} \tag{A.4}$$

$$2Z_0\frac{\Delta y H_y^{(n)}}{\bar{D}_y} = A_{my}\left[\left(\Delta z E_{10}^z + Z_{my}\Delta y H_{10}^y\right) - \left(\Delta z E_6^z - Z_{my}\Delta y H_6^y\right)\right]^{(n-(1/2))} \tag{A.5}$$

$$2Z_0\frac{\Delta z H_z^{(n)}}{\bar{D}_z} = A_{mz}\left[\left(\Delta x E_{12}^x + Z_{mz}\Delta z H_{12}^z\right) - \left(\Delta x E_1^x - Z_{mz}\Delta z H_1^z\right)\right]^{(n-(1/2))}. \tag{A.6}$$

Implicit part (from $n\Delta t$ to $(n+1/2)\Delta t$):

$$2\Delta x E_x^{(n)} = A'_{ex}\left[\left(\Delta x E_2^x - Z_{ex}\Delta y H_2^y\right) + \left(\Delta x E_9^x + Z_{ex}\Delta y H_9^y\right)\right]^{(n+(1/2))} \tag{A.7}$$

$$2\Delta y E_y^{(n)} = A'_{ey}\left[\left(\Delta y E_3^y - Z_{ey}\Delta z H_3^z\right) + \left(\Delta y E_{11}^y + Z_{ey}\Delta z H_{11}^z\right)\right]^{(n+(1/2))} \tag{A.8}$$

$$2\Delta z E_z^{(n)} = A'_{ez}\left[\left(\Delta z E_5^z - Z_{ez}\Delta x H_5^x\right) + \left(\Delta z E_7^z + Z_{ez}\Delta x H_7^x\right)\right]^{(n+(1/2))} \tag{A.9}$$

$$2Z_0\frac{\Delta x H_x^{(n)}}{\bar{D}_x} = A'_{mx}\left[-\left(\Delta z E_5^z - Z_{mx}\Delta x H_5^x\right) + \left(\Delta z E_7^z + Z_{mx}\Delta x H_7^x\right)\right]^{(n+(1/2))} \tag{A.10}$$

$$2Z_0\frac{\Delta y H_y^{(n)}}{\bar{D}_y} = A'_{my}\left[-\left(\Delta x E_2^x - Z_{my}\Delta y H_2^y\right) + \left(\Delta x E_9^x + Z_{my}\Delta y H_9^y\right)\right]^{(n+(1/2))} \tag{A.11}$$

$$2Z_0\frac{\Delta z H_z^{(n)}}{\bar{D}_z} = A'_{mz}\left[-\left(\Delta y E_3^y - Z_{mz}\Delta z H_3^z\right) + \left(\Delta y E_{11}^y + Z_{mz}\Delta z H_{11}^z\right)\right]^{(n+(1/2))}. \tag{A.12}$$

Second step:

Explicit part (from $(n+1/2)\Delta t$ to $(n+1)\Delta t$):

$$2\Delta x E_x^{(n+1)} = A_{ex}\left[\left(\Delta x E_2^x + Z_{ex}\Delta y H_2^y\right) + \left(\Delta x E_9^x - Z_{ex}\Delta y H_9^y\right)\right]^{(n+(1/2))} \tag{B.1}$$

$$2\Delta y E_y^{(n+1)} = A_{ey}\left[\left(\Delta y E_3^y + Z_{ey}\Delta z H_3^z\right) + \left(\Delta y E_{11}^y - Z_{ey}\Delta z H_{11}^z\right)\right]^{(n+(1/2))} \tag{B.2}$$

$$2\Delta z E_z^{(n+1)} = A_{ez}\left[\left(\Delta z E_5^z + Z_{ez}\Delta x H_5^x\right) + \left(\Delta z E_7^z - Z_{ez}\Delta x H_7^x\right)\right]^{(n+(1/2))} \tag{B.3}$$

$$2Z_0\frac{\Delta x H_x^{(n+1)}}{\bar{D}_x} = A_{mx}\left[\left(\Delta z E_5^z + Z_{mx}\Delta x H_5^x\right) - \left(\Delta z E_7^z - Z_{mx}\Delta x H_7^x\right)\right]^{(n+(1/2))} \tag{B.4}$$

$$2Z_0\frac{\Delta y H_y^{(n+1)}}{\bar{D}_y} = A_{my}\left[\left(\Delta x E_2^x + Z_{my}\Delta y H_2^y\right) - \left(\Delta x E_9^x - Z_{my}\Delta y H_9^y\right)\right]^{(n+(1/2))} \tag{B.5}$$

$$2Z_0\frac{\Delta z H_z^{(n+1)}}{\bar{D}_z} = A_{mz}\left[\left(\Delta y E_3^y + Z_{mz}\Delta z H_3^z\right) - \left(\Delta y E_{11}^y - Z_{mz}\Delta z H_{11}^z\right)\right]^{(n+(1/2))}. \tag{B.6}$$

Implicit part (from $(n+1)\Delta t$ to $(n+3/2)\Delta t$):

$$2\Delta x E_x^{(n+1)} = A'_{ex}\left[\left(\Delta x E_1^x + Z_{ex}\Delta z H_1^z\right) + \left(\Delta x E_{12}^x - Z_{ex}\Delta z H_{12}^z\right)\right]^{(n+(3/2))} \tag{B.7}$$

$$2\Delta y E_y^{(n+1)} = A'_{ey}\left[\left(\Delta y E_4^y + Z_{ey}\Delta x H_4^x\right) + \left(\Delta y E_8^y - Z_{ey}\Delta x H_8^x\right)\right]^{(n+(3/2))} \tag{B.8}$$

$$2\Delta z E_z^{(na+1)} = A'_{ez}\left[\left(\Delta z E_6^z + Z_{ez}\Delta y H_6^y\right) + \left(\Delta z E_{10}^z - Z_{ez}\Delta y H_{10}^y\right)\right]^{(n+(3/2))} \tag{B.9}$$

$$2Z_0\frac{\Delta x H_x^{(n+1)}}{\bar{D}_x} = A'_{mx}\left[-\left(\Delta y E_8^y - Z_{mx}\Delta x H_8^x\right) + \left(\Delta y E_4^y + Z_{mx}\Delta x H_4^x\right)\right]^{(n+(3/2))} \tag{B.10}$$

$$2Z_0\frac{\Delta y H_y^{(n+1)}}{\bar{D}_y} = A'_{my}\left[-\left(\Delta z E_{10}^z - Z_{my}\Delta_y H_{10}^y\right) + \left(\Delta z E_6^z + Z_{my}\Delta y H_6^y\right)\right]^{(n+(3/2))} \tag{B.11}$$

$$2Z_0\frac{\Delta z H_z^{(n+1)}}{\bar{D}_z} = A'_{mz}\left[-\left(\Delta x E_{12}^x - Z_{mz}\Delta z H_{12}^z\right) + \left(\Delta x E_1^x + Z_{mz}\Delta z H_1^z\right)\right]^{(n+(3/2))} \tag{B.12}$$

with

$$\bar{C}_i = \frac{s\Delta i}{\varepsilon_i \Delta j \Delta k} \text{ and } \bar{D}_i = \frac{s\Delta i}{\mu_i \Delta j \Delta k}$$

with

$$(i,j,k) \in \{(x,y,z),(z,x,y),(y,z,x)\}.$$

$$A_{ei} = \frac{4}{4+R_{ei}}$$
$$A'_{ei} = \frac{4}{4+R_{ei}}$$
$$R_{ei} = Z_0 s\frac{\sigma_{ei}}{\varepsilon_i}$$
$$Z_{ei} = Z_0\bar{C}_i$$

with

$$i \in (x,y,z).$$
$$A_{mi} = \frac{4}{4+R_{mi}}$$
$$A'_{mi} = \frac{4}{4-R_{mi}}$$
$$R_{mi} = s\frac{\sigma_{mi}}{Z_0\mu_i}$$
$$Z_{mi} = \frac{Z_0}{D_i}$$

with

$$i \in (x,y,z) \text{ and } s = 2c_0\Delta t.$$

ACKNOWLEDGMENT

The authors wish to acknowledge Dr. N. Peña, Universidad de Los Andes, Bogota, Colombia, for fruitful conversations on SS algorithms.

REFERENCES

[1] W. J. R. Hoefer, "The transmission-line matrix (TLM) method," in *Numerical Techniques for Microwave and Millimeter Wave Passive Structures*, T. Itoh, Ed. New York: Wiley, 1989.

[2] C. Christopoulos, "The transmission-line modeling method : TLM," in *IEEE/OUP on Electromagnetic Wave Theory*. Piscataway, NJ: IEEE Press, 1995.

[3] M. M. Ney and S. Le Maguer, "Diakoptics: An efficient technique for EMC applications," in *Proc. Electromagnetic Compatibility*, Zurich, Switzerland, 1999, pp. 339–342.

[4] P. B. Johns, "A symmetrical condensed node for the TLM method," *IEEE Trans. Microwave Theory Tech.*, vol. MTT-35, pp. 370–377, Apr. 1987.

[5] R. A. Scaramuzza and A. J. Lowery, "A hybrid symmetrical condensed node for the TLM method," *Electron. Lett.*, vol. 26, pp. 1947–1949, 1990.

[6] P. Berrini and K. Wu, "A pair of hybrid symmetrical condensed TLM nodes," *IEEE Microwave Guided Wave Lett.*, vol. 4, pp. 224–246, July 1994.

[7] V. Trenkic, C. Christopoulos, and T. M. Benson, "New symmetrical super-condensed node for the TLM method," *Electron. Lett.*, vol. 30, pp. 329–330, 1994.

[8] J. Rebel, T. Mangold, and P. Russer, "On the performance of TLM-SCN codes," in *Proc. 3rd Int. Transmission Line Matrix Workshop*, 1999, pp. 43–50.

[9] P. Russer and B. Bader, "The alternating transmission line matrix (ATLM) scheme," in *IEEE MTT-S Int. Microwave Symp. Dig.*, vol. 1, 1995, pp. 19–22.

[10] A. J. Wlodarczyk, "Representation of symmetrical condensed TLM node," *Electron. Lett.*, vol. 28, no. 18, pp. 1686–1687, Aug. 1992.

[11] P. Russer, "The alternating rotated transmission line matrix (ARTLM) scheme," *Electromagnetics*, vol. 16, pp. 537–551, 1996.

[12] T. Namiki, "A new FDTD algorithm based on alternating-direction implicit method," *IEEE Trans. Microwave Theory Tech.*, vol. 47, pp. 2003–2007, Oct. 1999.

[13] F. Zheng, Z. Chen, and J. Zhang, "Toward the development of a three-dimensional unconditionally stable finite-difference time-domain method," *IEEE Trans. Microwave Theory Tech.*, vol. 48, pp. 1550–1558, Sept. 2000.

[14] T. Namiki and K. Ito, "Numerical simulation using ADI-FDTD method to estimate shielding effectiveness of thin conductive enclosures," *IEEE Trans. Microwave Theory Tech.*, vol. 49, pp. 1060–1066, June 2001.

[15] S. L. Maguer and M. Ney, "Toward a new low-computer-cost 3D-TLM scheme (ADI-TLM)," in *Proc. 4th Int. Computational Electromagnetics in the Time Domain Workshop*, 2001, pp. 13–18.

[16] Y. M. Lee and C. C.-P. Chen, "Power grid transient simulation in linear time based on transmission-line-modeling alternating-direction-implicit method," in *Proc. Computer-Aided Design*, Nov. 4–8, 2001, pp. 75–80.

[17] ——, "Power grid transient simulation in linear time based on transmission-line-modeling alternating-direction-implicit method," *IEEE Trans. Computer-Aided Design*, vol. 21, pp. 1343–1352, Nov. 2002.

[18] K. S. Yee, "Numerical solution of initial boundary value problems involving Maxwell's equations in isotropic media," *IEEE Trans. Antennas Propagat.*, vol. AP-14, pp. 302–307, May 1966.

[19] G. I. Marchuk, "Splitting and alternating direction methods," in *Handbook of Numerical Analysis*, P. G. Ciarlet and J. L. Lions, Eds. Amsterdam, The Netherlands: North-Holland, 1990, vol. 1.

[20] N. Peña and M. M. Ney, "A general formulation of a three-dimensional TLM condensed node with the modeling of electric and magnetic losses and current sources," in *Proc. Applied Computational Electromagnetics Society*, 1996, pp. 262–269.

[21] S. Le Maguer and M. M. Ney, "Alterning TLM symmetrical condensed node," *Electron. Lett.*, vol. 38, no. 15, pp. 779–780, July 2002.

[22] M. Le Goff, J. L. Le Bras, B. Deschamps, D. Bourreau, and S. Toutain, "Focusing horn design for wideband quasioptical circuits measurements without time-gating," in *Proc. ESA Millimeter Wave Technology and Applications Workshop*, Espoo, Finland, 1998, pp. 269–274.

[23] S. Le Maguer, S. Guillou, and M. M. Ney, "PML absorbing conditions for a new SS TLM scheme," in *Proc. 5th Int. Computational Electromagnetics in the Time Domain Workshop*, Jun. 2003, pp. 1–6.
[24] A. Taflove, *Advances in Computational Electrodynamics*. Norwood, MA: Artech House, 1998, ch. 6.